LA-UR -87-2746

CONF-8708110--9

SEP 2 ...

Los Alamos National Laboratory is operated by the University of California for the United States Department of Energy under contract W-7405-ENG-36

LA-UR--87-2746

DE87 014722

TITLE **X-Ray Emission from High-Z Spherical Laser Plasmas: Implications for Plasma Dynamics**

AUTHOR(S) **P. D. Goldstone, J. A. Cobble, A. Hauer, G. Stradling, W. C. Mead, S. R. Goldman, & S. Coggeshall**
Los Alamos National Laboratory

M. C. Richardson, P. A. Jaanimagi, O. Barnouin, R. Marjoribanks, B. Yaakobi, F. J. Marshall, P. Auderbert, & J. Knauer
University of Rochester/LLE

SUBMITTED TO **SPIE Proceedings**
San Diego, CA

August 19-21, 1987

DISCLAIMER

Los Alamos Los Alamos National Laboratory
Los Alamos, New Mexico 87545

X-ray emission from high-Z spherical laser plasmas: Implications for plasma dynamics

P. D. Goldstone, J. A. Cobble, A. Hauer, G. Stradling, W. C. Mead, S. R. Goldman, S. Coggeshall

Los Alamos National Laboratory
Los Alamos, New Mexico 87544

M. C. Richardson, P. A. Jaanimagi, O. Barnouin, R. Marjoribanks, B. Yaakobi, F. J. Marshall, P. Audebert, and J. Knauer

University of Rochester
Laboratory for Laser Energetics
250 East River Road
Rochester, NY 14623

ABSTRACT

Conversion of 351-nm laser light to soft x-rays has been studied using spherical gold targets irradiated at 5 x 10^{12} - 4 x 10^{15} W/cm^2. Spectra and time histories of sub-keV and M-band emission are presented. Results have been compared to detailed models (LASNEX) to better determine the dynamics of the plasma processes which lead to x-ray emission.

I. INTRODUCTION

High-Z plasmas produced by short wavelength lasers in the ~10^{13} - 10^{15} W/cm^2 irradiance regime can radiate a large fraction of the total energy budget as soft x-rays, primarily <1.5 keV. This can be important for applications to inertial confinement fusion, where these x-rays may be used to indirectly drive the implosion of a fuel-filled capsule. In addition, both the line and continuum x-ray emission from these plasmas can have important applications to materials and biological research.

The x-ray emission from these plasmas results from a complex interplay of coupled processes including the laser absorption, thermal electron energy transport within the plasma, non-LTE (local thermodynamic equilibrium) atomic physics and radiation transport, and hydrodynamics. Model simulation of these plasmas typically requires a large radiation-hydrodynamics code such as LASNEX **(ref 1, Zimmerman)**. Tests of modeling predictions which are sensitive to these processes, together with spectroscopic studies, are important to developing an understanding and a predictive capability for x-ray emission.

One important prediction of LASNEX simulations is a change in the character of high-Z plasmas with laser intensity, from below I(lambda^2) = 10^{13} (W/cm^2)-um^2 to above that value. At low intensities, most of the laser light is absorbed by inverse bremsstrahlung in an extended region of the corona, and the rate of deposition is sufficiently low that radiation from the same extended region keeps the corona cool (<1 keV). At high intensities, the coronal temperature rises and most of the laser deposition occurs just below the critical density; electron thermal transport carries the energy to a narrow region of higher density just above critical, where the radiation takes place.

2. EXPERIMENTAL SETUP

The experiments described here **(ref 2, Goldstone)** were performed at the University of Rochester Omega laser **(ref 3, Soures)** frequency-tripled to 351 nm. Either the full 24 beam array or a 6-beam subset was used, but always with spherical symmetry. Pulses were nominally gaussian with a typical FWHM of 650 ps. Targets were solid polystyrene (CH) spheres coated with gold. Beams were focused beyond the target so that the edges of each beam were tangential to the target sphere, providing optimum irradiation uniformity (~50% rms for the six-beam series and ~20% rms for the 24-beam series). Intensities of 5×10^{12} – 4×10^{15} W/cm^2 were obtained by varying the target size at fixed laser energy (six beams, ~250 J; 24 beams, ~1.7 kJ). At 4×10^{13} and 4×10^{14} W/cm^2, both six- and 24-beam shots were performed. Different gold thicknesses, from 160 Angstrom to 3 um, allowed us to study emission in circumstances where the gold was completely ablated into the corona during the laser pulse, as well as for essentially infinite-thickness targets. Typical depths of laser burnthrough vary from <100 Angstrom to >1000 Angstrom over the intensity range we studied. For the remainder of this discussion we use the term "thick target" to describe those with gold thickness much greater than the laser burnthrough depth, and "thin target" to describe those with gold thickness less than or equal to the laser burnthrough depth.

Emission spectra were studied with a variety of crystal spectrographs covering 2 - 7 Angstrom, and a transmission grating spectrograph covering 2 - 140 Angstrom with 2 Angstrom resolution. In addition time-resolved spectra were obtained with a streaked grating spectrograph and a streaked elliptical crystal spectrograph (SPEAXS) **(ref 4, Jaanmagl)**. Absolute emission below 1.5 keV was inferred from a four-channel filtered x-ray-diode (XRD) spectrometer **(ref 5, Plen)**, using the grating spectra to provide detailed information as to the spectral shape. Plasma calorimeters were used to determine the laser absorption. To study the energy penetration into the thin-gold layered targets, we observed total x-ray conversion as a function of layer thickness as well as the time-resolved emission. The issue of extended coronal emission versus localized emission was studied in part by time-integrated keV x-ray microscopy and is also addressed by how abruptly the sub-keV emission decreases at the time of laser burnthrough into the CH substrate. Details of many of these x-ray diagnostics can be found in a recent review **(ref. 6, Richardson)**.

3. X-RAY CONVERSION (h(nu) < 1.5 keV)

For thick gold targets, x-ray conversion efficiencies $E_{radiated}/E_{absorbed}$ are shown in **Fig. 1**. A discussion of the data reduction may be found in reference 2. The agreement with LASNEX calculations is quite good for the high-energy, 24-beam data if essentially classical heat flux (flux limit f_c=0.08) is assumed. This flux limit is also consistent with thermal transport measurements in low-Z spherical experiments at short wavelength. Previous planar-target (disk) experiments had required inhibited heat flux (f_c=0.03) for adequate model fits **(ref.7, Mead)**.

Thus, for the 24-beam experiments the target energy balance appears to be well-modeled. The six-beam data, on the other hand, fall below the 24-beam conversion efficiencies and do not show the expected intensity dependence; they agree well with earlier low-energy disk data at the same laser wavelength **(ref. 8, Turner)**. The discrepancy between the six- and 24-beam data is particularly pronounced at ~3×10^{13} W/cm^2. While this discrepancy could imply a size- or laser-energy-dependence to the x-ray conversion not found in the model calculations, it is also possible that the reduced irradiation uniformity in the six-beam experiments plays a role.

4. LAYERED-TARGET BURNTHROUGH RESULTS

The time-integrated x-ray conversion (E_x < 1.5 keV) decreases for thin gold layers since the CH substrate is an ineffective x-ray emitter. The rate of decrease of the time-integrated emission with decreasing thickness, as well as the abruptness of the reduction in the time-resolved emission at the time of burnthrough, depend on the extent to which the emission is localized near the critical density or, conversely, comes from the extended corona. Time-integrated results (**Figure 2**) agree with modeling both in the thickness at which the emission begins to significantly decrease (indicating that the laser energy penetration or mass ablation is as calculated) and in the rate of decrease with thickness. Further discussion is found in reference 2.

Time-resolved sub-keV emission shows a rapid reduction at burnthrough time for 4 x 10^{14} W/cm^2 (**Figure 3**) consistent with the expected narrow emission region. At 4 x 10^{13} W/cm^2 (not shown), there is no such abrupt decrease in emission even for gold layers that are ablated early in the pulse; this is consistent with the emission coming from an extended region of the corona where the gold is present long after burnthrough. While there is a rapid emission decrease in Figure 3 as expected, it is apparent that in the 800-eV region there is considerably more emission after burnthough than calculated. From examinations of the streaked spectra this appears to be gold emission rather than carbon emission from the substrate. This may indicate more coronal emission than predicted by the model for this intensity. Also in **Figure 3**, note that the time history of M-band emission (~2-4 keV) as seen in the streaked grating spectrograph is not significantly affected by the layer thickness. This may be expected since these high-energy lines are most likely produced in the corona where the temperatures are highest. (However, one SPEAXS record in the M-band region did apparently show some emission-time shortening for a thin target.) M-band spectra and time histories are discussed further below.

5. SPATIAL DISTRIBUTIONS AND UNIFORMITY

Figure 4 shows 2-3 keV images from 24-beam irradiations, obtained with a Kirkpatric-Baez microscope. **Figure 4a** and **4b** are for thick gold layers at 4 x 10^{14} and 4 x 10^{15} W/cm^2 (initial target diameters of 450 um and 140 um), respectively. The images are highly limb-brightened, indicating a small optical thickness at this photon energy. The relatively uniform emission is apparent; in this intensity range the kilovolt emission varies approximately linearly with laser intensity **(ref. 9, Marshall)** and so this reflects the relatively uniform irradiation. Sub-kilovolt pinhole camera images also show relatively uniform emission from these targets. Some slight asphericity of the targets resulting from the fabrication process may be noted in figure 4.

Figure 4c is an image of a target with a 580-Angstrom-thick gold layer. For these thin layers we routinely observed a small-scale spatial modulation of the emission (of which **Fig. 4c** is a particularly dramatic example). This may be related to filamentation enhancing laser beam nonuniformities. Microscopic examinations of the uniformity of gold layer thickness on witness targets indicate that even these thin layers were uniform to ~10% down to micron-size areas. Thus gold thickness nonunformities would not appear to be a likely cause of this mottled emission pattern.

Figure 4d is an azimuthally-averaged lineout of **Fig. 4a** after conversion from film density to intensity. A comparison with a LASNEX/TDG calculation (normalized in intensity) shows that the calculated extent of the emission region and its motion with time during the laser pulse are reasonable.

6. SUB-KILOVOLT SPECTRA

Details of the sub-kilovolt continuum spectra differ significantly from the LASNEX calculations using non-LTE hydrogenic average-atom models, and also show interesting systematic changes with intensity, target size, and gold layer thickness. **Figure 5** shows a LASNEX-calculated spectrum and one obtained from the time-integrated grating spectrograph using 101 film and Henke's film calibration **(ref. 10, Henke)**. Note that the vertical scale is linear. The observed feature near 250 eV is attributed primarily to transitions into the gold O-shell (although (delta)n=0 transitions might also contribute to this region), and that near 600-800 eV is attributed to transitions into the N-shell (5-4 transitions). For simplicity we refer to these as the O- and N-band peaks, although this is not strictly correct.

Figure 6 shows spectra for thick and thin targets at intensities from 10^{13}-10^{15} W/cm^2. Note that the centroid of the N-manifold moves from ~600 eV to ~800 eV with increasing intensity, as the mean charge state of the emitting plasma increases from ~28 to ~50. This is consistent with LASNEX calculations. (The centroid of the N-band emission is at ~400 eV for 4 x 10^{12} irradiations, not shown). Also in **figure 6**, note that the thin-layered targets exhibit spectra with narrower O- and N- features; for thicker targets both broaden to the low-energy side.

Figure 7 shows a comparison of spectra from high-energy, large-target, 24-beam shots to those from lower-energy, small-target shots at the same intensity. The small-target thick-gold spectra are quite similar to those from large targets but thin gold layers. This suggests that the broadening to low energy seen in the large-target thick-layer shots may be related to an increased optical thickness of the plasma as compared to targets with less gold or smaller radius. We speculate that the apparent shift in x-ray conversion efficiency with target size and number of beams (**Fig. 1**) might be connected with such an effect, and we have attempted to reproduce a target-size dependence in x-ray conversion by adjusting various parameters within the LASNEX model, including oscillator strengths, opacity multipliers, line widths, and non-LTE rates. None of these changes had the desired effect, and we conclude that a more subtle improvement to the LASNEX model is needed to reproduce the spectral details and, perhaps, to reproduce the small-target x-ray conversion efficiencies.

7. M-LINE SPECTRA AND TIME HISTORIES

M-band (2-4 keV) emission is strongly dependent on laser intensity with relatively little emission below ~10^{14} W/cm^2, rising to several percent of the incident energy by 4 x 10^{15} W/cm^2. As much as 10-20% of the total radiated flux can be in M-band emission at these high intensities. A typical spectrum at ~10^{15} is shown in **Figure 8** along with identifications of several of the transition arrays. Typical ionization states responsible for this emission are Co-like to Ga-like (Z = 48 - 52).

Using SPEAXS to compare streaked M-band spectra with an optical fiducial, we find that the M-band emission is considerably delayed and shortened at the lower laser intensities. **Figure 9** shows overlays of the M-band emission and the optical fiducial for two shots, one at 4 x 10^{13} and one at 4 x 10^{15} W/cm^2. At the lower intensity the onset of M-emission is delayed by ~110 ps. The shortening and delay of keV line emission is physically reasonable, since the emission will have a strong dependence on the coronal temperature for these relatively cold plasmas and will only be significant near the peak of the laser heating pulse.

8. CONCLUSIONS

We have found that in kilojoule-scale experiments with good uniformity of irradiation, x-ray conversion is efficient and the overall target energy balance agrees well with the LASNEX modeling. From the layered-target burnthrough experiments and imaging, it is apparent that the calculated laser energy penetration and the gross hydrodynamic motion of the target, along with the spatial characteristics of the sub-keV emitting region (localized or extended), are in reasonable agreement with experimental results. For smaller targets in lower energy experiments with poorer uniformity, x-ray conversion is reduced, particularly at low intensity. The origin of this effect is not clear and future experiments will attempt to distinguish between the effects of uniformity and target-size scaling. Average-atom calculations do not well reproduce details of the emission spectra, although the shift in the centroid energy of the N-band emission is consistent with the calculated variation of mean charge state in the emitting region. More detailed atomic physics models will be required to calculate these spectral features and their observed changes with gold layer thickness and target size. Finally, M-band emission can contain several percent of incident laser energy at the highest intensities studied here.

9. ACKNOWLEDGEMENTS

The authors thank the target fabrication group at Los Alamos and the Omega operations team for their important contributions to this work. In addition we would like to acknowledge continuing valuable discussions with R. Kauffman, B. Lasinski, L. Suter, and J. Delettrez. This work was supported by the U. S. Department of Energy, Office of Inertial Fusion, and at Rochester by the University of Rochester Laser Fusion Feasibility Project

10. REFERENCES

1. G. B. Zimmerman, Lawrence Livermore National Laboratory report No. UCRL-75881, 1974 (unpublished); G. B. Zimmerman and W. L. Kruer, "Numerical simulation of laser-initiated fusion," Comments Plasma Phys. Controlled Fusion 2, 51-61 (1975)

2. P. D. Goldstone et al., "Dynamics of high-Z plasmas produced by a short-wavelength laser," Phys. Rev. Lett. 59, 56-59 (1987)

3. J. M. Soures et al., "Omega: a short wavelength laser for fusion experiments," in Proceedings of the Tenth Symposium on Fusion Engineering, C. C. Hopkins, D. M. Pulyer, J. N. Stacy, and K. E. Wakefield, eds., IEEE, New York, 1392 (1983)

4. B. L. Henke and P. A. Jaanimagi, "Two-channel, elliptical analyzer spectrograph for absolute, time-resolving time-integrating spectrometry of pulsed x-ray sources in the 100-10,000-eV region," Rev. Sci. Instr. 56, 1537-1552 (1985)

5. G. Pien, M. C. Richardson, P. D. Goldstone, R. H. Day,F. Ameluri, and G. Eden, "Computerized 3-GHz multi-channel soft x-ray diode spectrometerfor high density plasma diagnosis," Nucl. Instr. and Meth. B18, 101-110 (1986)

6. M. C. Richardson et al., "Time-resolved x-ray diagnostics for high density plasma physics studies," in Laser Interaction and Related Plasma Phenomena, v. 7, H. Hora and G. Miley, eds., Plenum, New York, 179-211 (1986)

7. W. C. Mead et al., "Laser irradiation of disk targets at 0.53 um wavelength," Phys. Fluids 26, 2316-2331 (1983)

8. R. E. Turner et al., "X-ray conversion at 1(omega), 2(omega), and 3(omega)," in Lawrence Livermore National Laboratory report No. UCRL-50021-81, pp. 6-34 - 6-35, unpublished (1982)

9. F. J. Marshall, et al., "Uniformity of direct-drive laser illumination measured by x-ray imaging," 17th Anomalous Absorption conference, Tahoe City, CA (1987)

10. B. L. Henke, F. G. Fujiwara, M. A. Tester, C. H. Dittmore, and M. A. Palmer, "Low-energy x-ray response of photographic films. II. Experimental characterization," J. Opt. Soc. Am. B1, 828-849 (1984)

Figure captions

1. Thick-target x-ray conversion efficiency

2. Fraction of thick-target x-ray emission as a function of gold thickness

3. Experimental and calculated time histories of x-ray emission for thick (left) and thin (right) targets at 4×10^{14} W/cm^2. Streak camera has ~15 ps resolution, XRD ~300 ps. All streaks are normalized to peak intensity, but the two XRD records are on a common absolute scale.

4. 2-3 keV images of target emission. 4a-4d (top left to bottom right) explanation in text.

5. Calculated and experimental sub-keV spectra at 4×10^{14} W/cm^2. Vertical scale is linear.

6. Spectra from thick (solid lines) and thin (dotted lines) targets at different intensities.

7. Comparison of kilojoule thick-target spectra to both thin-target and low-energy/small-target spectra.

8. Gold M-band spectrum at 10^{15} W/cm^2

9. SPEAXS comparison of M-band emission and optical fiducial

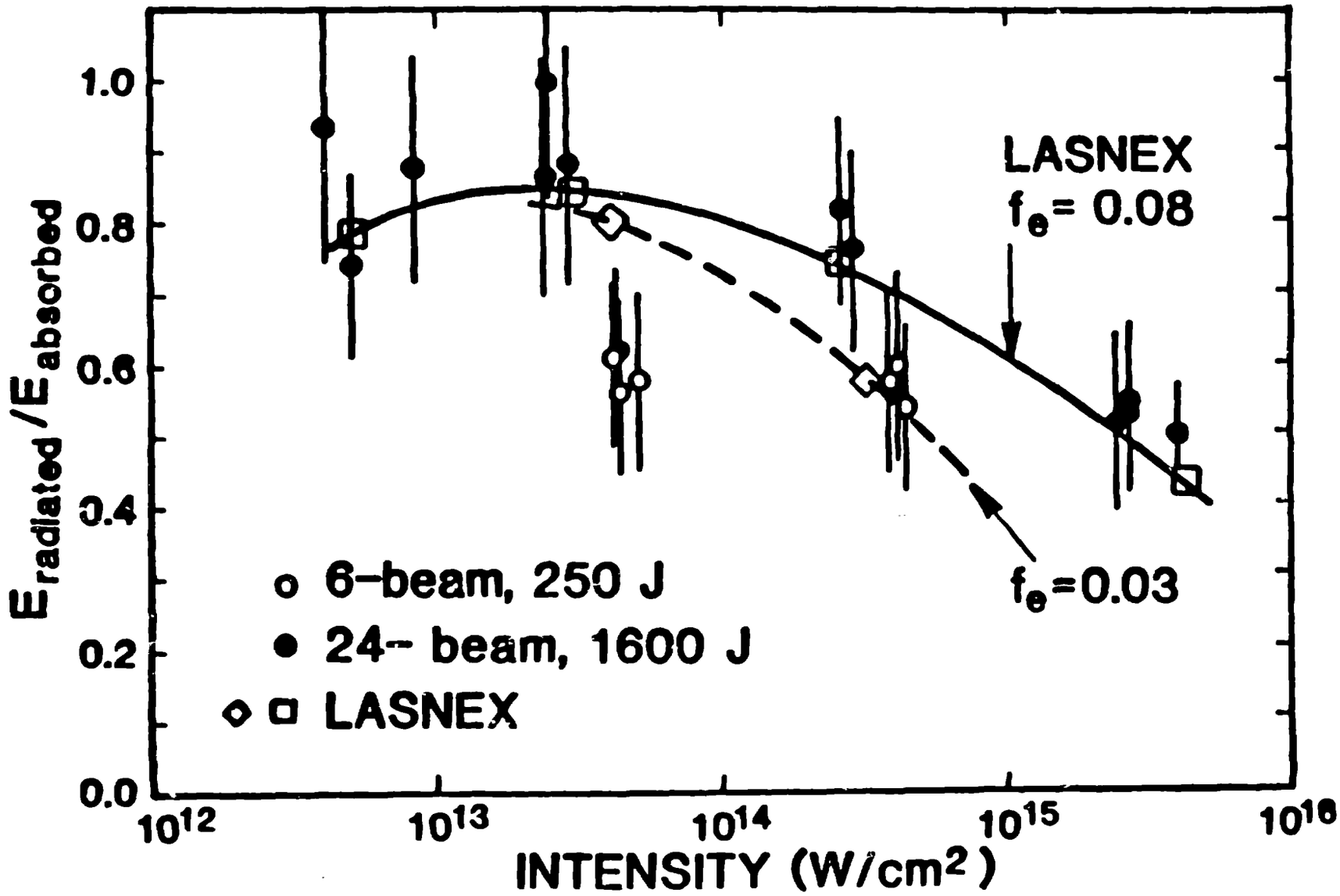

Figure 1
P. D. Goldstone, et al.

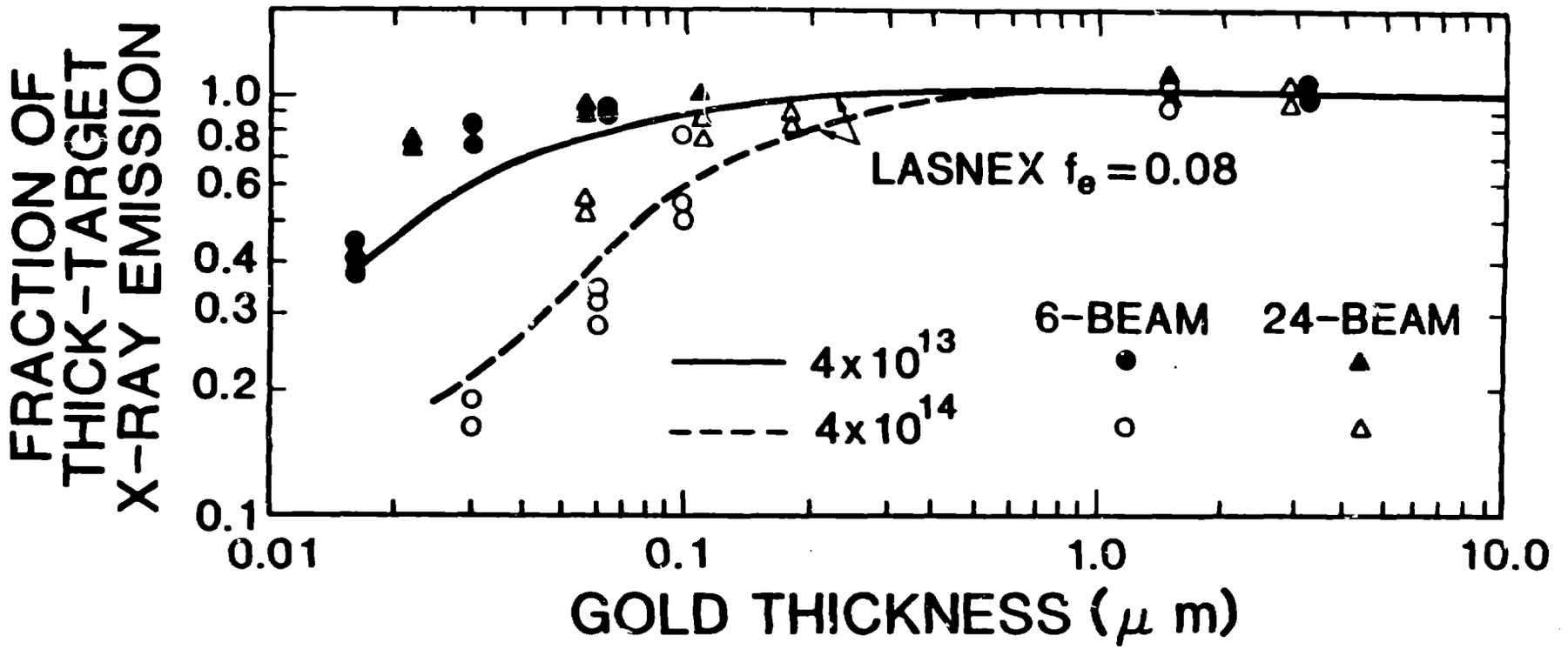

Figure 2
P. D. Goldstone, et al.

Fig 2

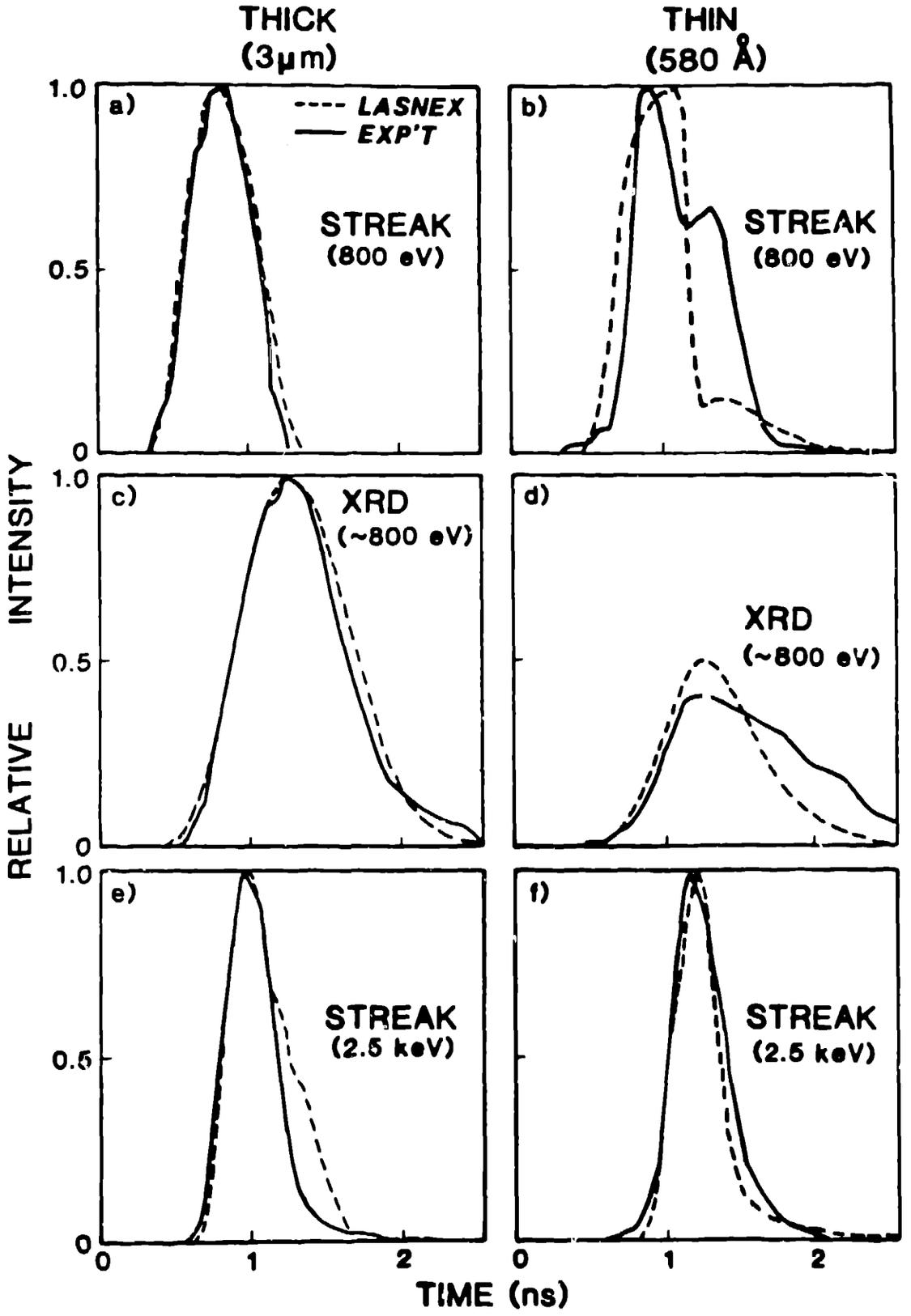
THICK
(3μm)
THIN
(580 Å)
a)
---- LASNEX
—— EXP'T
STREAK
(800 eV)
b)
STREAK
(800 eV)
c)
XRD
(~800 eV)
d)
XRD
(~800 eV)
e)
STREAK
(2.5 keV)
f)
STREAK
(2.5 keV)
RELATIVE INTENSITY
1.0
0.5
0
0
1
2
TIME (ns)

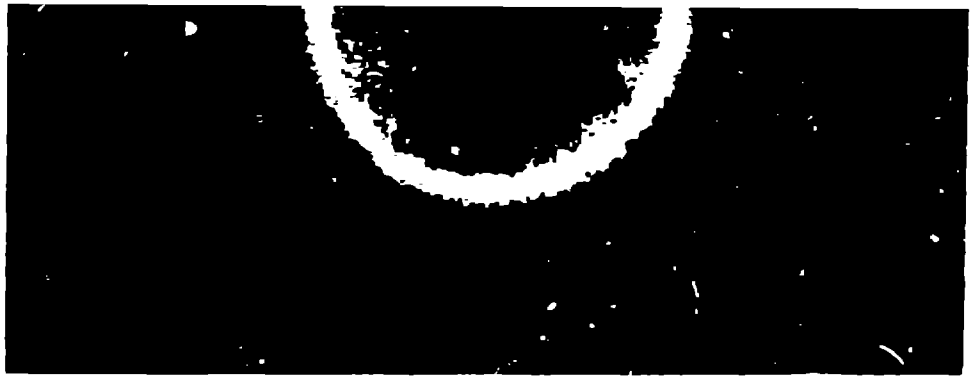

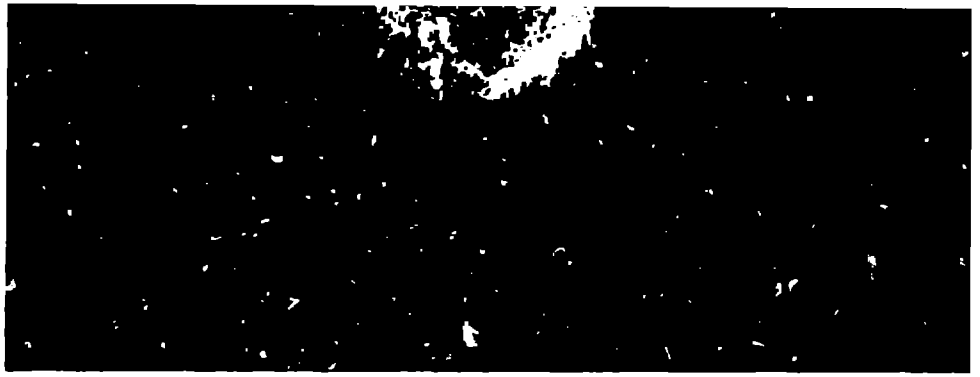

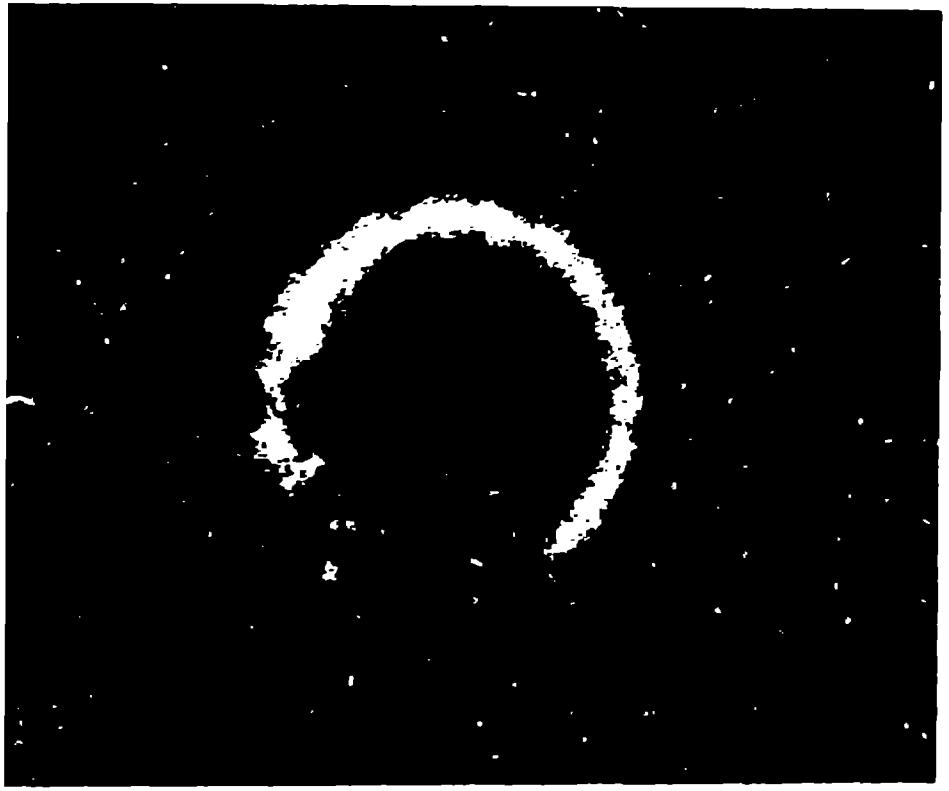

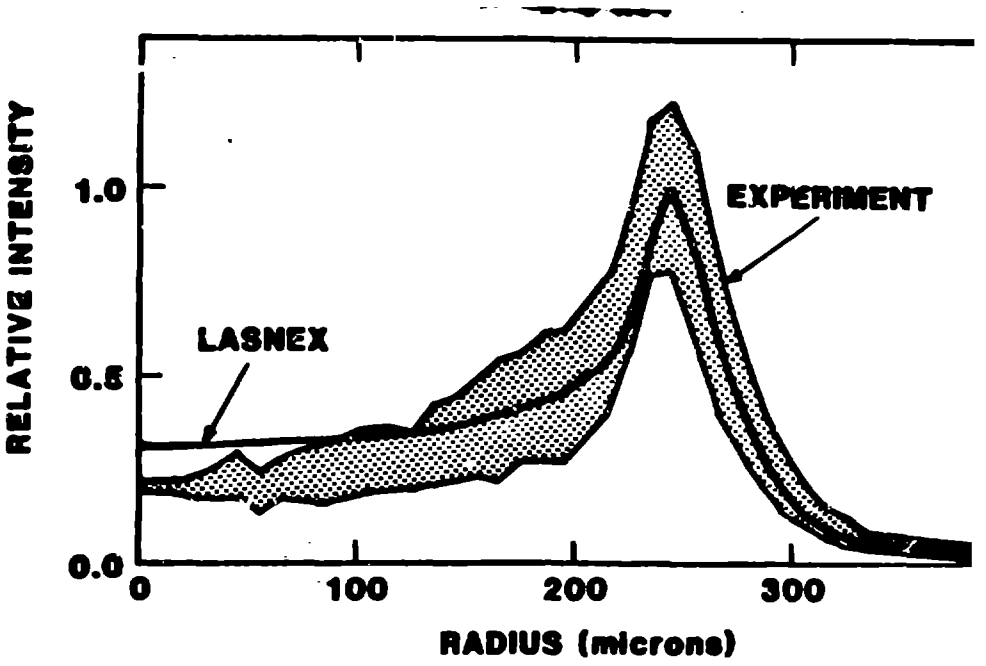
RELATIVE INTENSITY
1.0
0.5
0.0
0
100
200
300
RADIUS (microns)
LASNEX
EXPERIMENT

F 15

LIMB EMISSION EXTENT AND RELATIVE BRIGHTNESS AGREE WELL WITH CALCULATIONS

4×10^{14} W/cm^2, 600ps

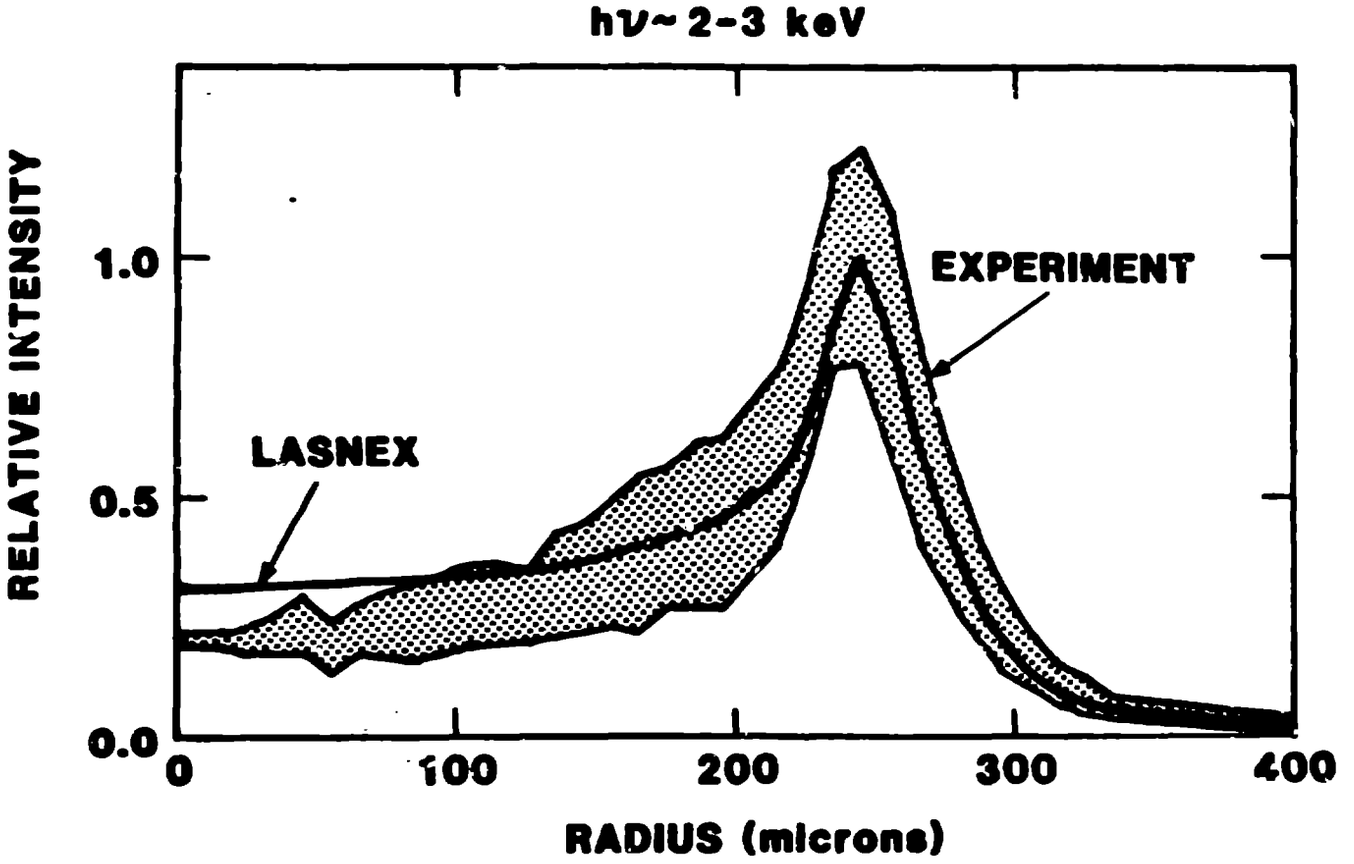

- Calculated localization of x-ray emission reasonable

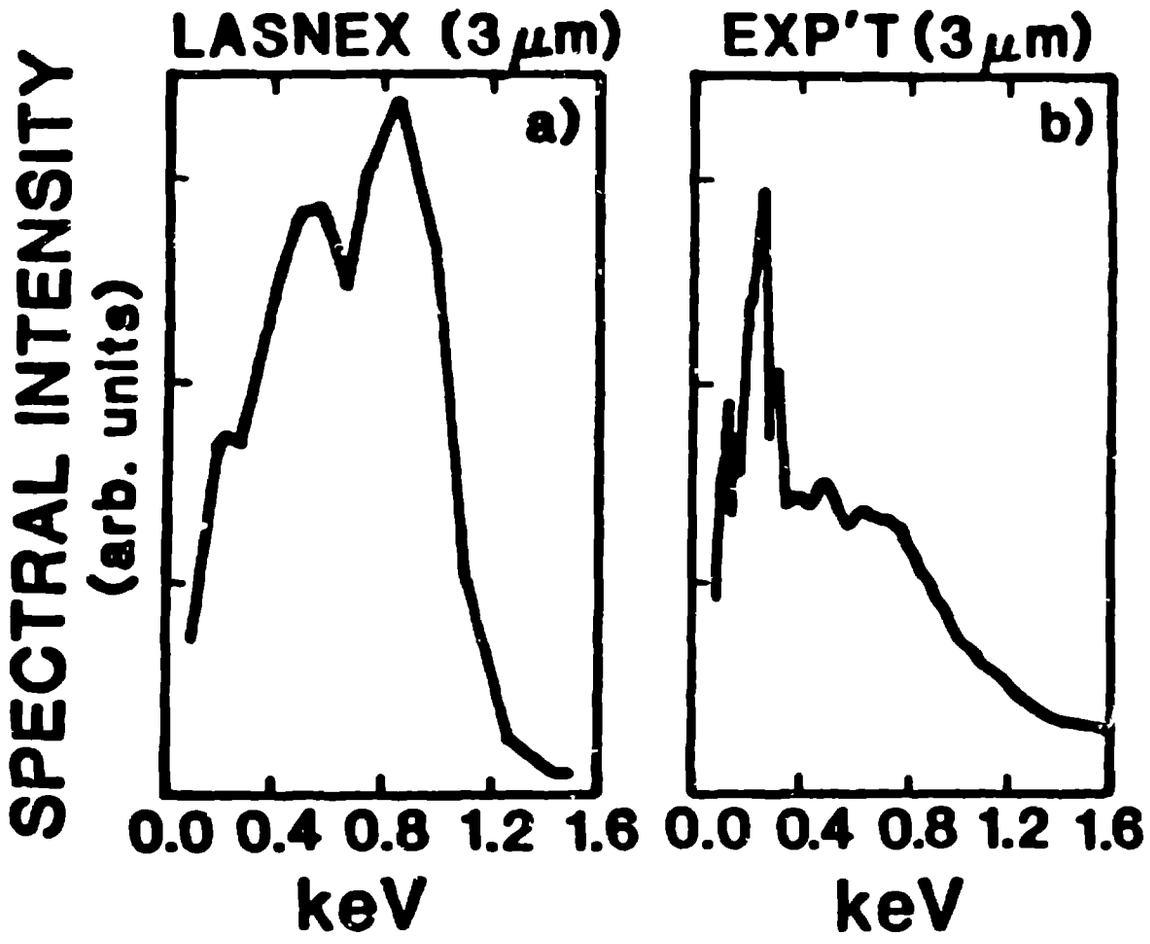

Figure 4
P. D. Goldstone, et al.

Fig 5

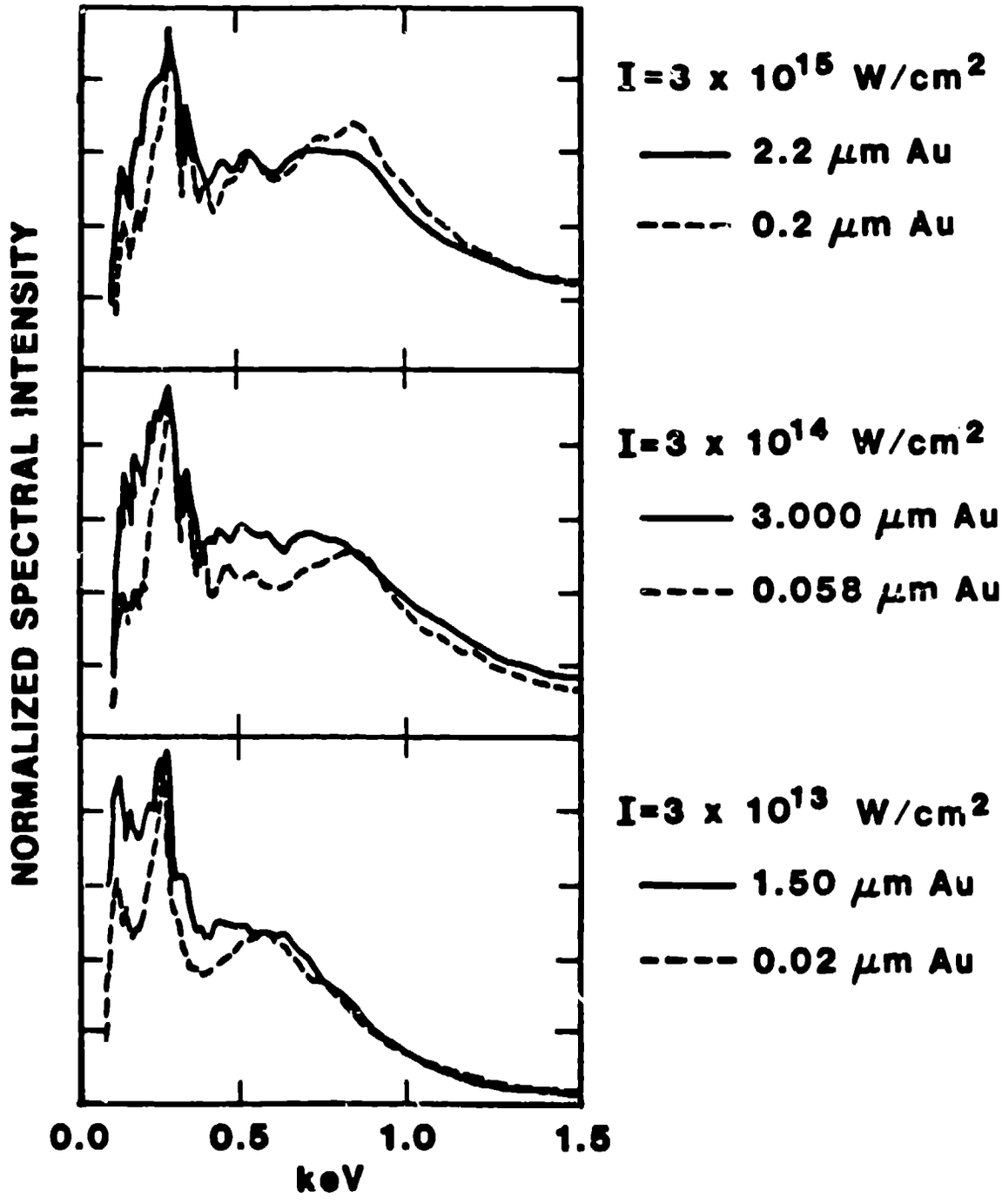
NORMALIZED SPECTRAL INTENSITY
0.0
0.5
1.0
1.5
keV
I=3 x 10^15 W/cm^2
2.2 μm Au
0.2 μm Au
I=3 x 10^14 W/cm^2
3.000 μm Au
0.058 μm Au
I=3 x 10^13 W/cm^2
1.50 μm Au
0.02 μm Au

SMALL, LOW-ENERGY SHOTS PRODUCE SPECTRA SIMILAR TO THOSE FROM THIN GOLD LAYERS

Narrower "O" peak, more pronounced "N" peak for smaller/thinner targets

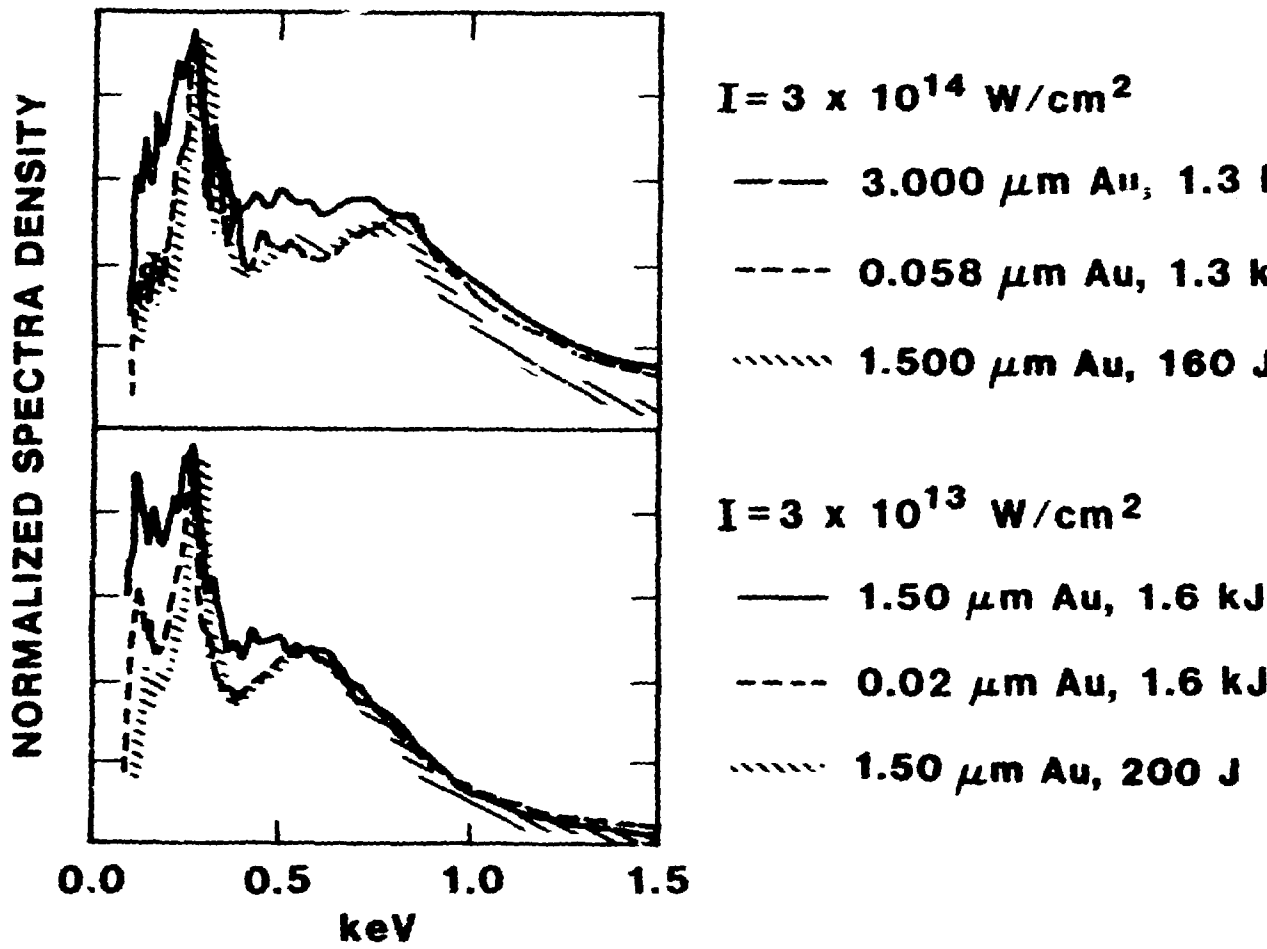

Fig 7

GOLD M-BAND SPECTRUM AT 10^{13} W/CM^2

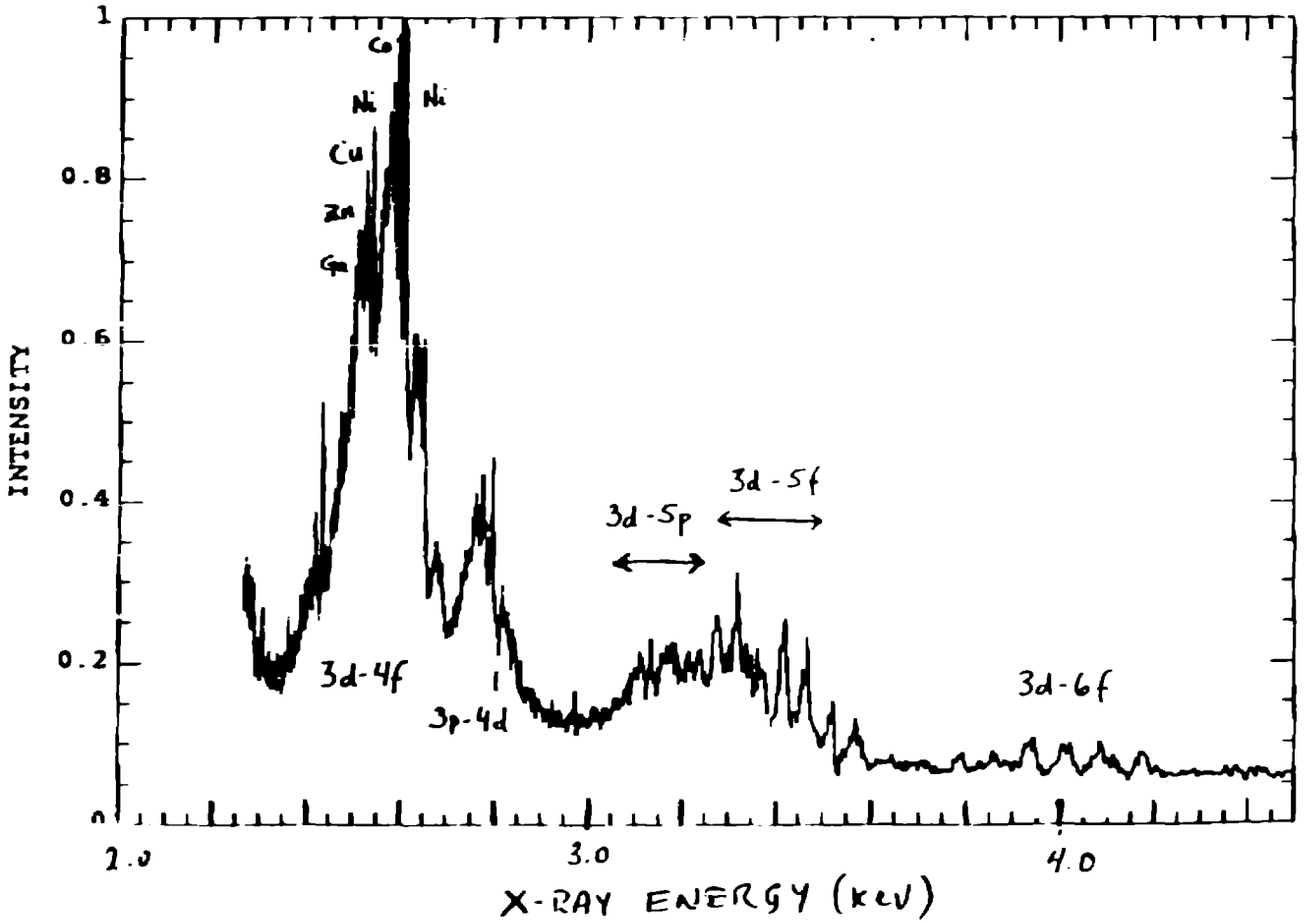

Fig 3
(no logo)

SPEAXS COMPARISON OF M-BAND EMISSION AND OPTICAL FIDUCIAL SHOWS DELAYED ONSET AT LOW INTENSITY

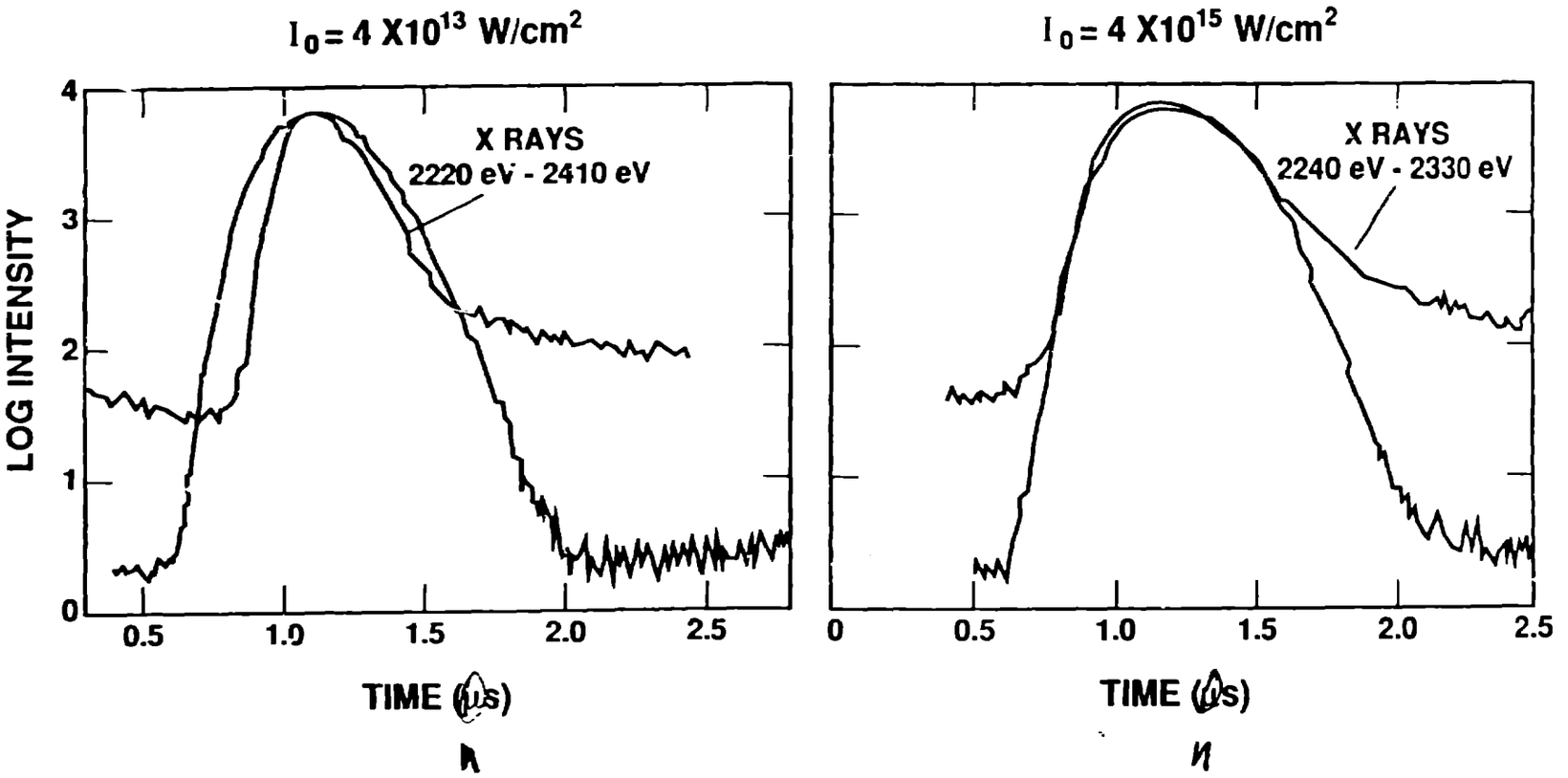

Fig 9